PANEL METHOD CACULATIONS OF WING - TAIL INTERFERENCE EFFECTS

Asst. Lec. Maki H. Majeed
University of Baghdad., College of Engineering, Mechanical Eng. Dept.

ABSTRACT

A low-order panel method was used to predict the flow characteristics between two sets of wings representing wing and tail. Constant source and doublet singularities with Drichlet boundary condition are used on the body surfaces. Distance and setting angle changes of the tail are studied to predict the air flow characteristics. Since the flow is incompressible non-viscous (potential flow), the results obtained contain a large physical evidence and may give a good design tool for aircraft stability consideration. A **FORTRAN** program was built to calculate the flow characteristics and then validated with published data. Highly acceptable results are obtained as compared with these data, so that; the program can be used for discussing the design or control parameters of such aerodynamical problems.

الخلاصة

طريقة الالواح ذات الدرجة الواطئة استخدمت لتخمين خواص الجريان مابين جناحين يمثلان الجناح والذنب. استخدم مصدر وقطب مع تطبيق شرط دريشلت على سطح الجسم. تغيير البعد وزاوية التثبيت للذنب تمت درستها لتخمين خواص جريان الهواء. رغم ان الجريان لا انضغاطي وغير لزج (جريان كامن)، فان النتائج المتحصلة منه كانت تحمل الكثير من الملاحظات الفيزيائية والتي من الممكن ان تكون اداة جيدة لدراسة استقرارية الطائرات. برنامج بلغة الفورتران تم بناءه لحساب خواص الجريان وتحقيق هذه النتائج مع بيانات منشورة. النتائج المتحصلة كانت مقبولة الى حد عالي مع هذه البيانات المنشورة، ولذلك فان البرنامج يمكن استعماله لمناقشة عوامل التصميم والسيطرة لمسائل الديناميكا الهوائية.

KEYWORDS: Wing-Body-Tail Interference, Potential Flow, Panel Method

INTRODUCTION

While the present work is dealt with the interference between wing and tail, it could be regarded as lifting surface –vortex interference. Vortices passing close to a lifting surface can cause significant changes in the aerodynamics characteristics of the lifting surface. An important example is the loss of tail effectiveness, which results from wing vortices pass in close proximity to the tail. **Fig (1)** shows the physical situation that give rise to such wing tail interference.

Changing the wing and tail angle of attack is very effective aspect of controlling the airplane. For the design aspect, the distance between the wing and tail, their shapes and sizes would make a large change in aerodynamics of the airplane.

If complete configuration without the wing is first considered the tail wing will then develop lift that is mostly generated by the tail and tail body interference. The addition of wing to the previous configuration will cause a general down wash field in the region of tail

panels, and thereby reduces their lifting effectiveness. The loss of tail lift can be directly ascribed to the modification of the flow field produced by the vortices shed by the wing. It is clear that any vortices regardless of their origin will in passing close to the tail produced interference effect similar to those produced by the wing vortices.

Several methods were established to investigate the flow field behavior upon and around bodies moving inside fluids. The researchers always try to implement numerical methods that solve engineering problems with a satisfactory agreement with experimental data. This led to introduction of the panel method, which is reliable potential solution for a wide range of a complex geometries compared with actual measured data. Articles on this method were published since 1967 up to date which indicate the justification of such method in the field of aerodynamic design.

Many previous works studied the interference problem between different parts of airplanes like wing-body-tail components. Most of these studies used panel method as a tool to analyze the interference problem due to simplest form of this method and its ability to deal with complex configuration. The first beginning with **(Hess and Smith 1967**) used the panel method in solving the problem of lifting and non-lifting bodies by distribution of constant sources and vortices on them. Neuman boundary condition was used with kutta condition to find the strength of these singularities .The flow is incompressible and the results were in good agreement with both analytical and experimental data, the method still to be an efficient tool in aerodynamic problems especially on the interaction between air plane components like wing, body and tail components. After them **(Morino and Kuo 1974)** present a general method for steady and unsteady linearized subsonic flow around arbitrary shape. A distribution of constant source strength with constant doublet was used with the Drichlet boundary condition. **(Morino 1975**) extend this method for linearized supersonic flow. These results for different body's interactions agree well with experimental data and available exact solution of selected bodies. (**Tinoco 1984)** use higher order panel method represented by **PANAIR** commercial program to predict complex configuration like wing-body-tail. Good results are obtained as compared with experimental data.

(Bandyo pahyay 1989) developed a numerical method to calculate the aerodynamic characteristics of wing-canard configurations by considering both the attached and separated flow over the canard surface using horse-shoe vortex technique. Experimental test have been conducted in a low Speed wind tunnel to compare the theoretical results. The comparison shows good agreement up to 16^o incidences.

(Arnott and Berstin 2000) made an analysis for aerodynamic interference at the forward swept wing and plate interaction region with a fully developed turbulent boundary layer. Flow visualization and surface pressure distribution have been made for Reynold Number 1.03×10^6 based on the wing chord and free stream velocity equal 30m/s. For low stall angles, boundary layer separation was wake at plate while a higher angles many separation regions have been noticed with a large three-dimensional vortex region.

The present work deals with the aerodynamic characteristics of wing and tail interaction in low speed region. Wing wake is considered to be a flat vortex sheet and the reaction of the tail section is then calculated. Low-order panel method is used to predict the flow characteristics due to complex shapes and incompressible potential flow were assumed for the flow.

PANEL METHOD FORMULATION

Panel method is commonly used for analyzing subsonic and supersonic inviscid flows about Configurations of arbitrary geometries, and is widely use throughout the areo-space industry. A major advantage of panel methods is that they are not encumbered by the need for a field grid for numerical solution, and as thus free of most of the geometric limitations which today limit the non-linear method to simpler configuration **(Katz and Plotkin 1999).**

The flow outside the boundary layer is assumed to be incompressible, besides it is irrotational. The continuity equation in terms of the potential function (Φ) is:

$$\nabla^2\Phi = 0 \tag{1}$$

The general solution of equation (1) can be constructed by assuming a source (σ) and doublet (μ) distribution placed on the boundary of the body assigned as (s);

$$\Phi = \phi_\infty + \frac{1}{4\pi}\int_s \left[\mu\,\hat{n}\times\nabla\left(\frac{1}{r}\right) - \sigma\left(\frac{1}{r}\right)\right]ds \tag{2}$$

Where ($\hat{n}$) is the normal vector on the surface (s) and in the direction of the potential (μ) and (ϕ_∞) is the free stream potential;

$$\phi_\infty = Q_{l\infty}x + Q_{m\infty}y + Q_{n\infty}z \tag{3}$$

If the wake of the body is modeled with a doublet **eq. (2)** will be;

$$\Phi = \frac{1}{4\pi}\int_{body+wake}\mu\,\hat{n}\times\nabla\left(\frac{1}{r}\right)ds - \frac{1}{4\pi}\int_{body}\nabla\left(\frac{1}{r}\right)ds + \phi_\infty \tag{4}$$

The boundary condition of **eq. (1)** can directly be specified as zero normal velocity component $\left(\partial\Phi/\partial n\right)$=0 on the surface (s) in which case this direct formulation is called the Neuman problem. It is possible to specify the potential (Φ) on the boundary, so that the zero normal flow condition will be met, this is called Drichlet problem. The second boundary condition are used, so that; the distributing of singularity elements on the surface and placing the point (x, y, z) inside the surface (s) the inner potential (Φ_i) in terms of the surface singularity distributions is obtained;

$$\Phi_i = \phi_\infty + \frac{1}{4\pi}\int_{B+W}\mu\,\hat{n}\times\nabla\left(\frac{1}{r}\right)ds - \frac{1}{4\pi}\int_{b}\nabla\left(\frac{1}{r}\right)ds \tag{5}$$

B+W means body and wake surface. For enclosed boundary e.g. (s), $\left(\partial\Phi/\partial n = 0\right)$ as required by the boundary condition of zero normal velocity ($\nabla\left(\phi_p + \phi_\infty\right)\times\hat{n} = 0$) then the potential inside the body (without internal singularities) will not change **(Katz and Plotkin 1999)**.

$$\boldsymbol{\Phi_i = const.} \tag{6}$$

Now let the source be;

$$\sigma = \vec{Q}_\infty \bullet \hat{n} \tag{7}$$

Then **eq. (5)** can be written as;

$$\frac{1}{4\pi}\int_{B+W}\mu\hat{n}\times\nabla\left(\frac{1}{r}\right)ds-\frac{1}{4\pi}\int_{B}\sigma\left(\frac{1}{r}\right)ds=0 \tag{8}$$

NUMERICAL SOLUTION

The body is divided into NB surface panels and NW wake panels. The Drichlet boundary condition will be specified at each body panel at a "collocation point" which for the Drichlet boundary condition must be specified inside the body. In most cases though, the point may be left on the surface without moving it inside the body.

$$\sum_{K=1}^{NB}\frac{1}{4\pi}\int_{B}\mu\hat{n}\times\nabla\left(\frac{1}{r}\right)ds+\sum_{L=1}^{NW}\frac{1}{4\pi}\int_{W}\mu\hat{n}\times\nabla\left(\frac{1}{r}\right)ds-\sum_{K=1}^{NB}\frac{1}{4\pi}\int_{B}\sigma\left(\frac{1}{r}\right)ds=0 \tag{9}$$

Element of constant source strength (σ) and doublet strength (μ) are assumed thus, **eq. (9)** can be written as;

$$\sum_{k=1}^{NB}c_k\mu_k+\sum_{l=1}^{NW}c_l\mu_l+\sum_{K=1}^{NB}B_K\sigma_K=0 \tag{10}$$

Where the result of integration for a quadrilateral panel can be found in **(Katz and Plotkin 1999**) as;

$$C_k=\frac{1}{4\pi}\int_{panel}\frac{\partial}{\partial\hat{n}}\left(\frac{1}{r}\right)ds_k$$

$$B_k=\frac{1}{4\pi}\int_{panel}\left(\frac{1}{r}\right)ds_k \tag{11}$$

The source strength of (σ) is selected from **eq. (7),** then the coefficients (B_k) are known and can be moved to the right side of the **eq. (10)** by using Kutta condition, the wake doublet can be expressed as follows;

$$\mu_w=\mu_u-\mu_l \tag{12}$$

So that the **eq. (10)** can be simplified as follows:

$$C_w\mu_w=C_w(\mu_u-\mu_l) \tag{13}$$

$$\sum_{k=1}^{NB}A_k\mu_k=-\sum_{K=1}^{NB}B_K\sigma_K \tag{14}$$

Where

$A_K=C_K$ If the panel not at T.E

$A_K=C_K\pm C_W$ If the panel is at T.E

It could be written in matrix notation as;

$$[A]\{\mu\} = -[B]\{\sigma\} \tag{15}$$

AERODYNAMIC LOADS

Once **eq. (15)** is solved and the unknown singularities values are obtained; the velocity components are evaluated from local coordinate's derivation, the two tangential perturbation velocities are;

$$q_l = \frac{\partial \mu}{\partial l} \tag{16}$$

$$q_m = \frac{\partial \mu}{\partial m} \tag{17}$$

Where the differentiation is made numerically using the values on the neighbor panels, the normal component of the velocity is obtained from the source

$$q_n = -\sigma \tag{18}$$

The total velocity in the local direction of panel (k) is

$$Q_K = \left(Q_{\infty L}, Q_{\infty m,} Q_{\infty n}\right) + \left(q_l, q_{m,} q_n\right) \tag{19}$$

The pressure coefficient can be computed at each panel using panel Bernaullies equation;

$$C_{pk} = \frac{p_k - p_\infty}{\frac{1}{2}\rho_\infty Q_\infty^2} = 1 - \frac{Q_K^2}{Q_\infty^2} \tag{20}$$

The total aerodynamic forces are calculated from

$$F_x = -\frac{1}{2}\rho_\infty Q_\infty^2 \sum_{k=1}^{NB} C_{pk} A_k n_{xk}$$

$$F_z = -\frac{1}{2}\rho_\infty Q_\infty^2 \sum_{K=1}^{NB} C_{pk} A_k n_{zk} \tag{21}$$

Where A_k = area of each body panel and n_{xk}, n_{zk} = Component of unit normal vector ($\hat{n}$) in X and Z directions.

The lift and induced drag forces are calculated by:

$$F_l = F_z \cos\alpha - F_x \sin\alpha$$

$$F_D = F_z \sin\alpha + F_x \cos\alpha \tag{22}$$

The moment at reference point is;

$$M = 0.5\rho Q_\infty^2 \left[\sum_{k=1}^{NB} \left(C_p A n_x\right)_k (Z_{ck} - Z_{ref}) + \left(C_p A n_z\right)_k (X_{ck} - X_{ref}) \right] \tag{23}$$

In which $(X_{ck,}Z_{ck})$ are the global coordinates of each collocation point and (X_{ref}, Z_{ref}) are the reference moment point of the body.

A combination between rectangular wing and tail in potential flow is patterned by changing the space between them and the angle of setting of the tail as shown in **Fig (2).** The interference between the wing and tail can be clearly seen from the pressure coefficient distribution along the mid stream line on wing and tail and from dynamic forces on them. The other parameter like wing and tail aspect ratio and cross-sectional airfoil are selected constant for all cases studied in the present work.

It must be noted that the wake will be assumed straight (flat wake shape) and deflected with an angle of attack of the wing, to prevent wake to go inside tail which may cause an error in pressure distribution on the tail due to presence of singularity inside it, so that; there will be difference in height level between them. This approximation is done in real case where most of aircraft place the tail at higher or lower level from wing position and never placed in the same level.

The procedure discussed in the numerical method is used to build a computer program in Fortran 90 power station and modified to predict complex configurations like wing-body-tail system. To insure that program give reasonable results, the program results must be verified with other dependent published results.

RESULTS AND DISCUSSION

Figs (5, 6, 7, and 8) show a comparison between the present code and the results of software program called **PANAIR** pilot code **(Tinoco 1984)** which is a commercial potential flow program predicts subsonic and supersonic flow over complex bodies. The discretization of a selected case (swept back tapered wing) is shown in **Figs (3 and 4).** Also the control point is clear in **Fig (4).** Other figures **(5, 6, 7 and 8)** show pressure distribution (upper and lower surfaces) on the wing surface of two angles of attack and two span wise stations**.** Good agreement between present works with pilot code is clear.

To simplify the interference between wing and tail problem the consideration will be concentrated on some parameters like the distance between them and the tail setting angle. Wing and tail is considered as a rectangular wings as shown in **Fig (9)** where all the dimensions are assumed with respect to chord length of the wing. The reference area and length which is used in calculation of the aerodynamic coefficients are calculated with respect to wing area and its chord length. Also **Fig (9)** shows the discretized wing and tail configuration, it is seen that dense panels are used at leading and trailing edge for both wing and tail. This type of discretization is used due to rapid change in flow characteristics at these regions and it gives approximately constant aspect ratio for each panel.

Fig (10) illustrates the influence of tail on the wing by considering the lift coefficient distribution along the span of wing with tail and without tail at 5^o angle of attack. The figure shows the influence of tail on the wing which clearly increasing the load slightly on it. Pressure distribution on the wing surface is shown in figures (**11 and 12).** A comparison with tailness wing shows no major difference between them. The figures shows small tail effect on the wing and it could be neglected.

Fig (13) shows that lift distribution along the tail. Two cases are studied, the first consideration predicts the tail without wing at angle of attack of 5^o where a free stream goes on its surface and the other consideration the effect of wing on the tail is considered. The difference is clearly shown in the figure, by decreasing the lift distribution along the span wise of the tail. The decreasing in lift could be represented by decreasing in angle of attack at tail. The down wash behind the wing acted as a normal velocity in the down ward direction which tries to decrease the angle of attack on the tail.

Fig (14) shows a comparison between lift distribution along the span of wing and tail at 5^o angle of attack. It is clear that the wing carry most of lift and the tail used mainly to control. Pressure distribution on the tail surface with and without wing is shown in **Figs (15 and 16)**. The figures show a difference in two cases, which lead to a difference in load on the tail.

An important figure which illustrates the relation between wing and tail effect is shown in **Fig (17)** where lift coefficient is considered with and without interference between them. The most important notice that is the wing load increased due to presence of tail while tail load decrease from tail alone due to presence of wing. The overall wing tail load shows an increase in lift coefficient with angle of attack for them. **Fig (18)** shows another notice for them, the figure illustrates that the induced drag coefficient decreased for wing and tail simultaneously due to interference effect on wing and tail with that when take them alone.

Fig (19) represents the stability curve of the wing-tail system, because it represents a relation between moment coefficient variations with lift coefficient. The figure constructed from four curves representing wing-tail combination and wing moment alone. The reference moment point is located at 0.5 of wing chord length behind wing leading edge. It could be seen that the wing moment tends to cause a positive moment coefficient at a reference point. While the tail causes a reverse action on this point, the figure is separated with a vertical line at zero moment coefficients to illustrate the stability behavior. Due to large lift produced on the wing as compared with tail, the moment of the system (wing-tail) tend to be a positive behavior i.e. nose up. This mean the system is not stable i.e. at the right side of the figure and the inclination of the overall curve is positive as clearly illustrated in the figure.

To consider a different parameter and its effects on the system which contain wing and tail, the distance and setting angle of the tail is illustrated in foregoing discussion. The distance of the tail from the wing increased gradually from the wing to consider the interference effect between them. **Fig (20)** shows this effect by considering the lift coefficient on the tail and wing. Clearly there is no major effect on the lift coefficient with increasing the distance. But **Fig (21)** shows an increasing in the induced drag of the wing as the tail goes far from the wing, and this satisfied **Fig (18)** which illustrates that the induced drag of the wing without tail is larger than that with tail. The far distance means that there is no effect between two set of wings.

Fig (22) is an important graph where the moment coefficient vs. distance between wing and tail is presented at angle of attack 5^o. The moment coefficient changes its behavior as the tail reached to a distance equal approximately to 3.56 of wing chord length measured from wing leading edge to the leading edge of the tail. At this position the stability is satisfied and the moment tends to make a nose down for the wing-body system.

Other parameter considered here is the setting angle of the tail. This angle is added or subtracted to the angle of attack of the wing and tail system. **Fig (23)** shows the lift coefficient of the wing and tail, it could be seen that the lift coefficient of the tail increased rapidly with the setting angle of the tail while the wing lift coefficient is constant with this angle. The overall lift coefficient increased with this angle as shown in figure.

Fig (24) shows that the increasing in induced drag due to increasing in the tail induced drag. The other notice is the wing induced drag which is decreased due to interference effect as it is clear in the figure.

Fig (25) shows the wing will be stable at angle of attack equal to 3.5^o approximately. The tail is stable for all setting angle which overcome the unstable wing moment coefficient.

CONCLUSIONs

The results show that there is an interference causing a change in longitudinal characteristics of each wing and tail. The increase distance between wing and tail decrease the

interference effect and increase the stability of wing-tail system. It is found also that for the system suggested in the present work the moment stability occurred at distance 3.5 times wing chord make the system stable. The results can be seen in the transport aircraft where the tail at a far distance from wing. The increasing of setting angle of tail will cause an increasing in stability of wing-tail system. The interaction between them causes an increasing in lift coefficient for the whole system (wing and tail) also in the induced drag. The moment coefficient prediction shows that the system will be stable at 3.5^o setting angle of tail. These results could be applied in military aircraft where the length of aircraft is small.

REFERENCES

- **Arnott A. D. and Berstein L.,** "Aerodynamic Interaction at the Junction Between A forward Swept Wing and Plate," Aeronautical Journal, Vol. 104, No. 1023, 2000.
- **Bandyopadhyay G.,** "Low-Speed Aerodynamics of Canard Configurations," Aeronautical journal, January 1989.
- **Hess J. L., and Smith A. M. O.,** "Calculation of Potential Flow about Arbitrary Bodies," Progress in Aeronautical Science Journal, Vol. 8, Pergamon Press 1967.
- **Katz J. and Plotkin A.,** "Low Speed Aerodynamics From Wing Theory To Panel Method," McGraw Hill, 1999.
- **Morino L., and Kuo C.,** "Subsonic Potential Aerodynamic for Complex Configuration: A General Theory," AIAA journal, Vol. 12, No. 2, 1974.
- **Morino L., Chen L. T., and Emil O. Suciu,** "Steady and Oscillatory Subsonic and Supersonic Aerodynamics around Complex Configuration," AIAA journal, Vol. 13, No. 3, 1975.
- **Tinoco E. N.,** "PANAIR Analysis of Supersonic/Subsonic Flow about Complex Configurations," the University of Tennessee Space Institute, Tullahoma, Tenessee 37388, March 1984.

NOMENCLATURE

A	Panel Area	m^2
A	Doublet influence matrix	
AR	Aspect ratio	
B	Source influence matrix	
b_w b_T	Wing and Tail Span	m
c	Wing Chord length	m
c_T	Tail Chord Length	m
C_l	Section Lift Coefficient	m
C_L	Total Lift Coefficient	m
C_m	Pitching Moment Coefficient	m
C_p	Pressure Coefficient	

F_D	Drag Force	N
F_L	Lift Force	N
F_x	Axial Force	N
F_z	Normal Force	N
l, m, n	Local directional unit	
M	Moment	N.m
n_x,n_y,n_z	Normal direction unit	
NW	Number of Division on the wake	
NB	Number of division on the body	
Q	Total velocity	m/s
x_{ref}, z_{ref}	Reference point	m
x_t	Distance between wing and tail leading edge	m
α	Angle of attack	Deg
ϵ	Tail Setting Angle	Deg
Φ	Total velocity potential	$m^2/2$
μ	Doublet Strength	$m^2/2$
μ_w	Doublet Strength of wake	$m^2/2$
Φ_∞	Free Stream Velocity Potential	$m^2/2$
σ	Source Strength	$m^2/2$
ρ_∞	Free Stream Density	Kg/m^3

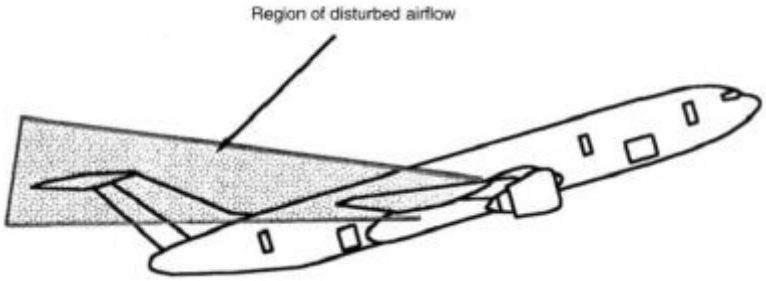

Fig (1): Interaction Problem Between Wing and Tail in Flying Aircraft.

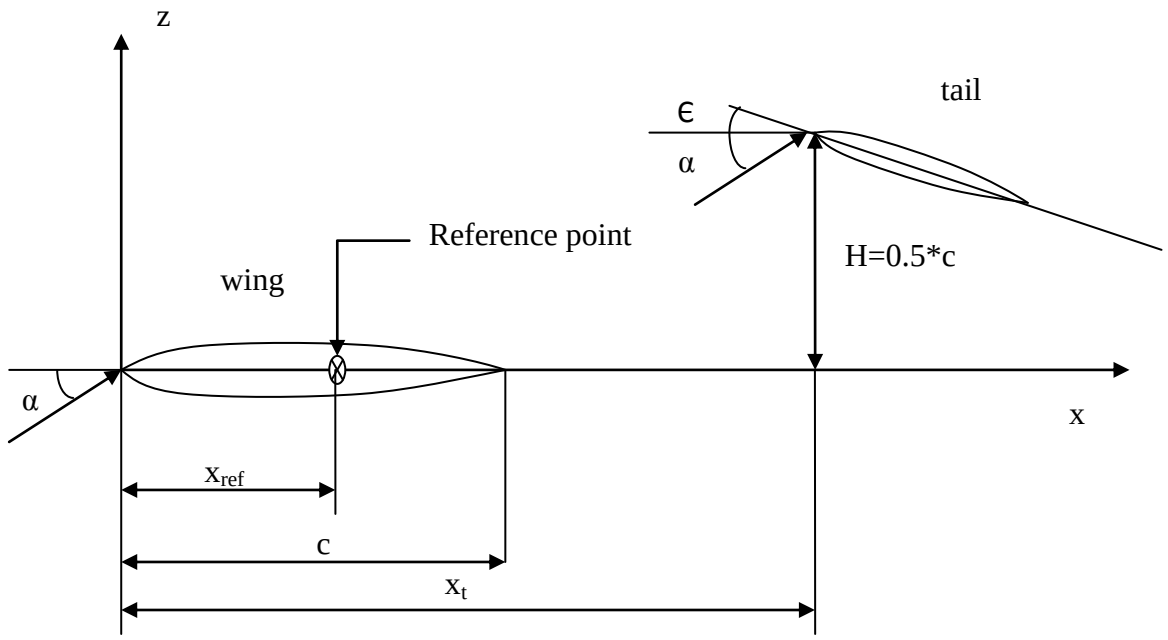

Fig (2): Terminology of Wing-Tail Interaction Problem.

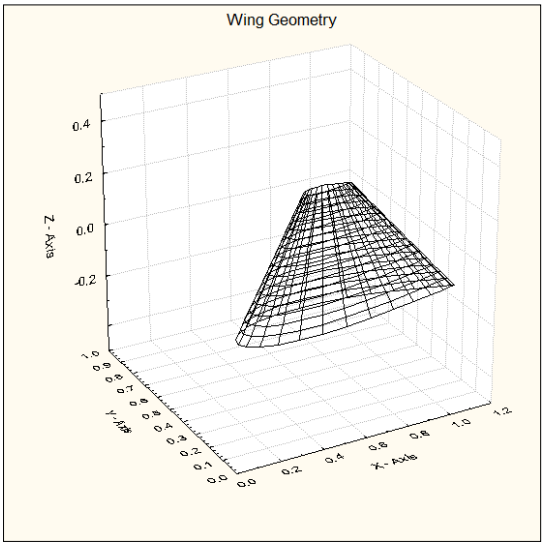

Fig (3): Wing Geometry.

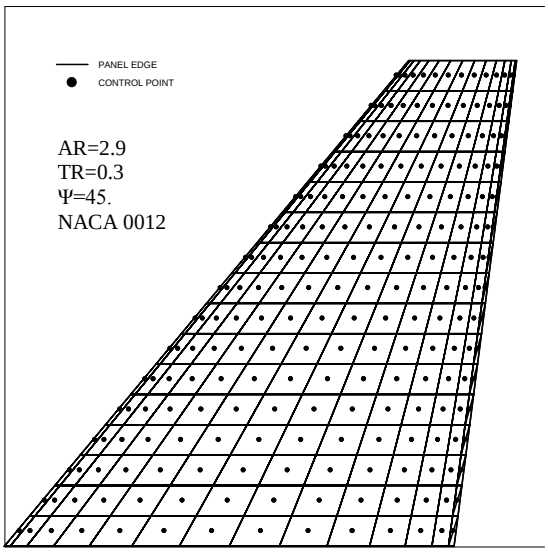

Fig (4): Wing Panels and Control Point.

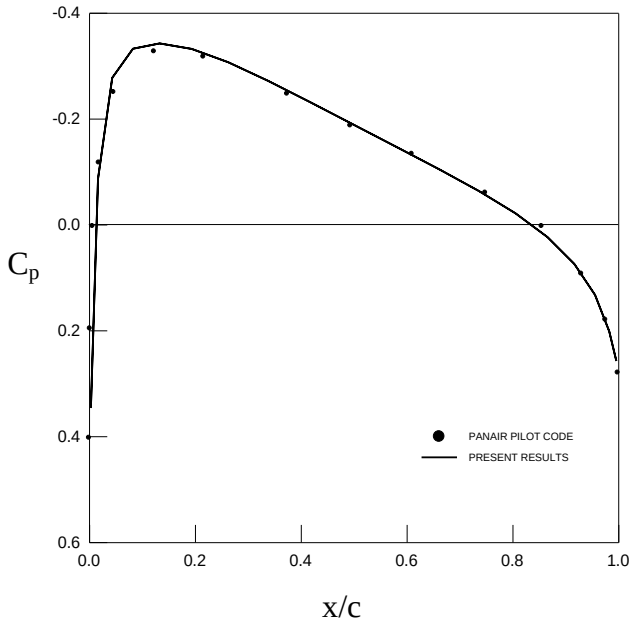

Fig (5): Pressure Distribution at 2y/b=0.19 and α=0.

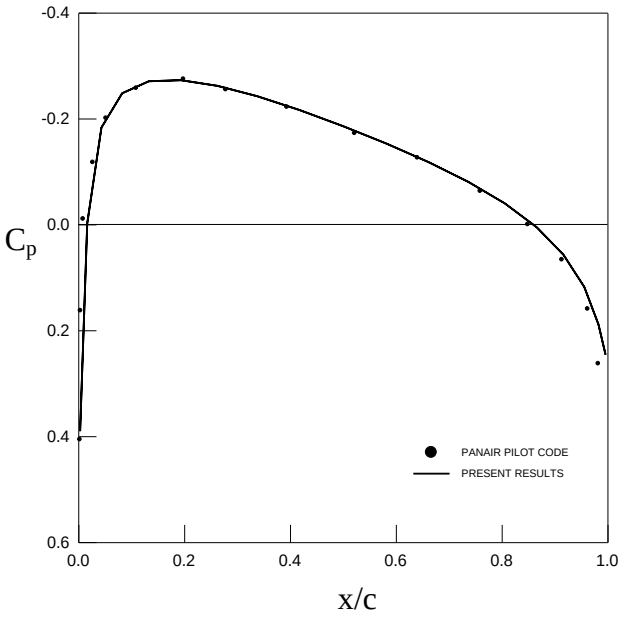

Fig (6): Pressure Distribution at 2y/b=0.81 and α=0.

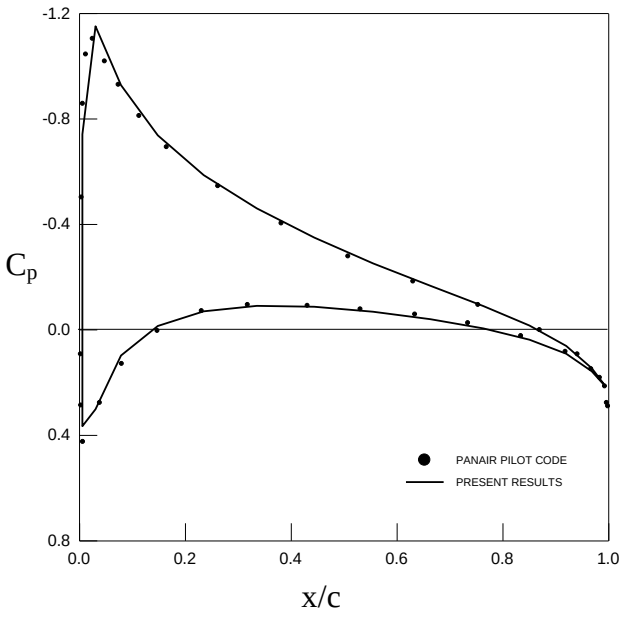

Fig (7): Pressure Distribution at 2y/b=0.19 and $\alpha=5^o$.

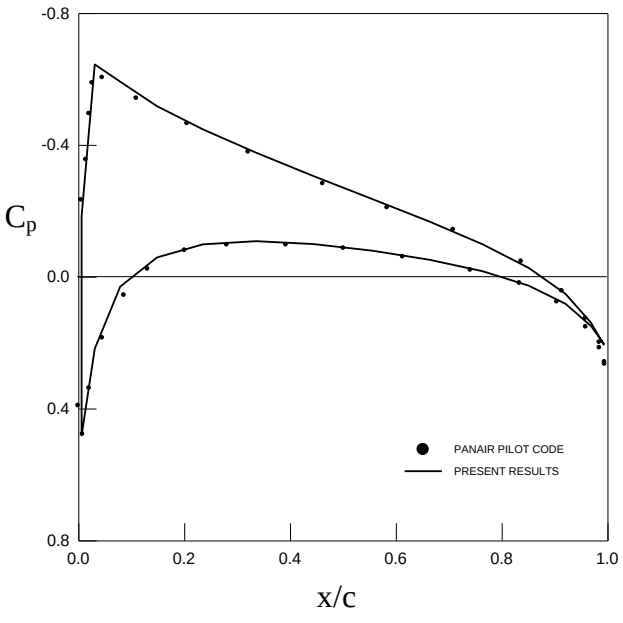

Fig (8): Pressure Distribution at 2y/b=0.81 and $\alpha=5^o$.

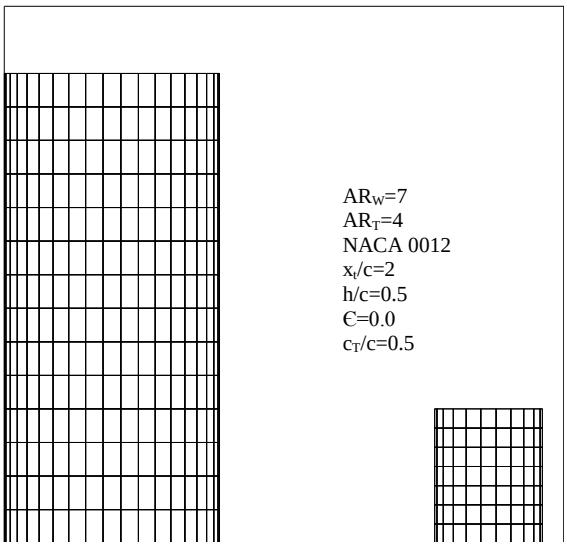

Fig (9): Wing-Tail Geometry.

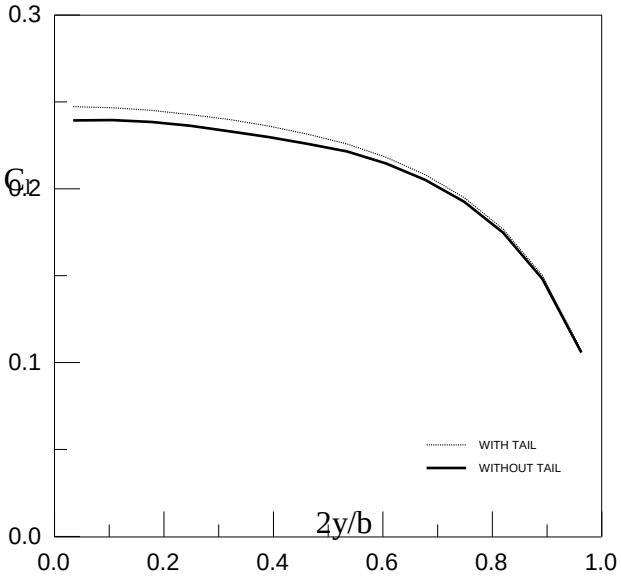

Fig (10): Lift Distribution along Span Wise Direction of Wing

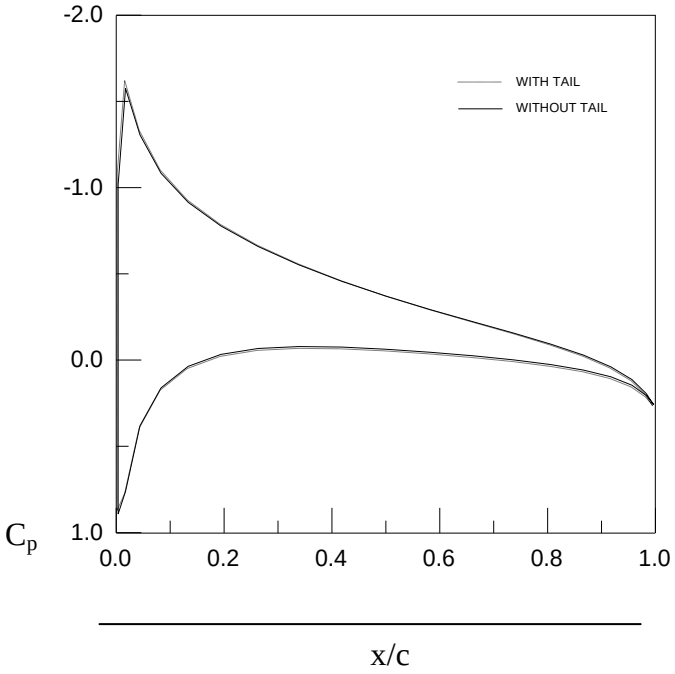

Fig (11): Pressure Distribution on the Wing at 2y/c=0.19.

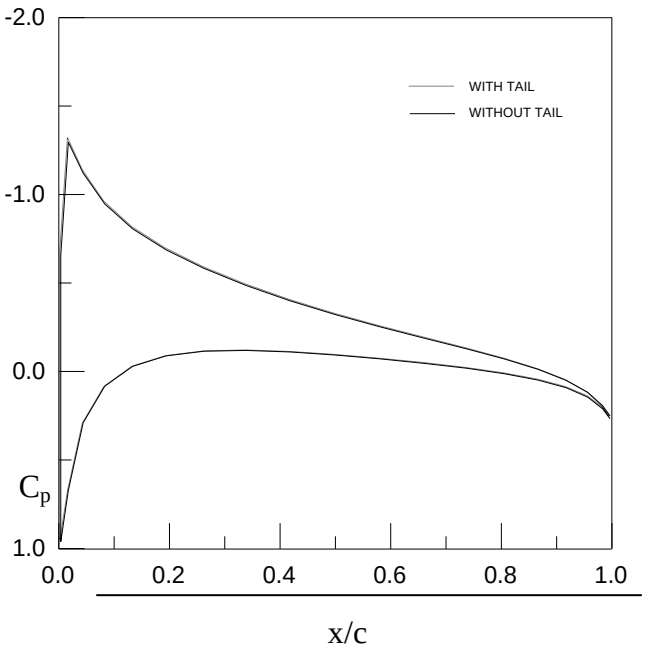

Fig (12): Pressure Distribution on the Wing at 2y/c=0.81.

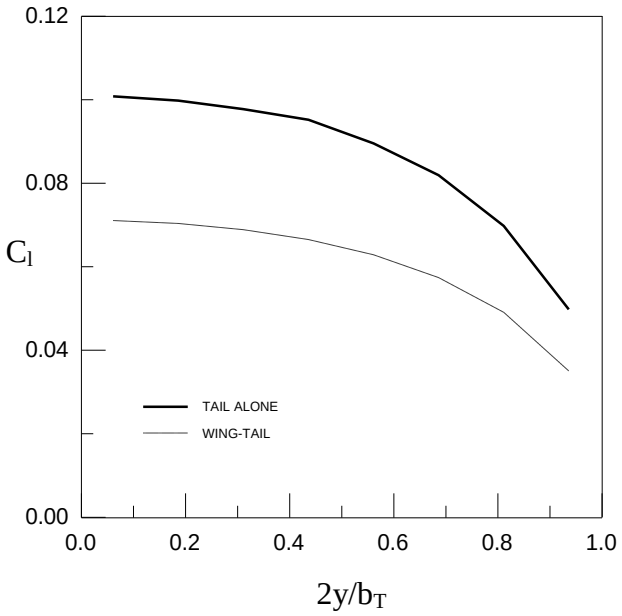

Fig (13): Lift Distribution a Long Span Wise Direction of Tail $\alpha=5^o$.

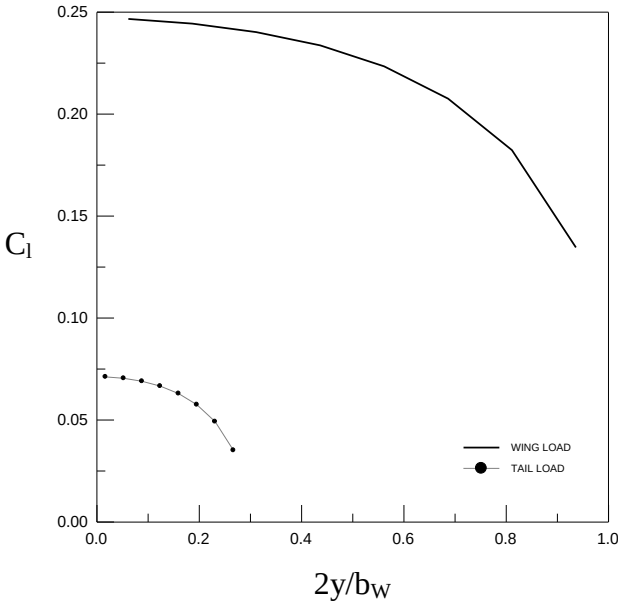

Fig (14): Lift Distribution a Long Span Wise Direction for Wing and

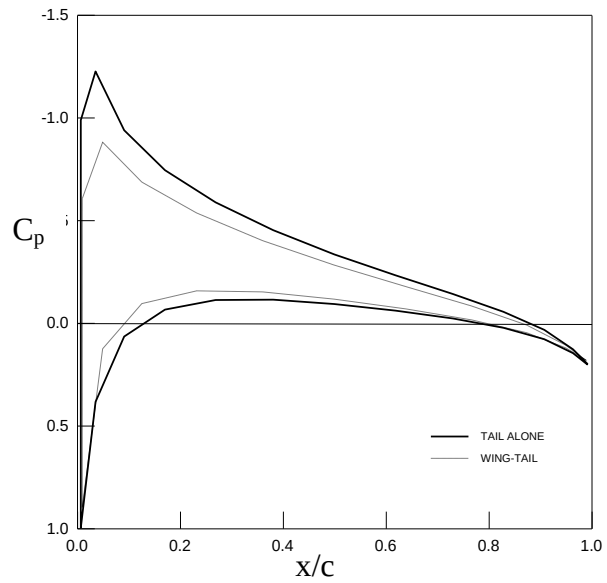

Fig (15): Pressure Distribution on the Tail at 2y/c=0.19.

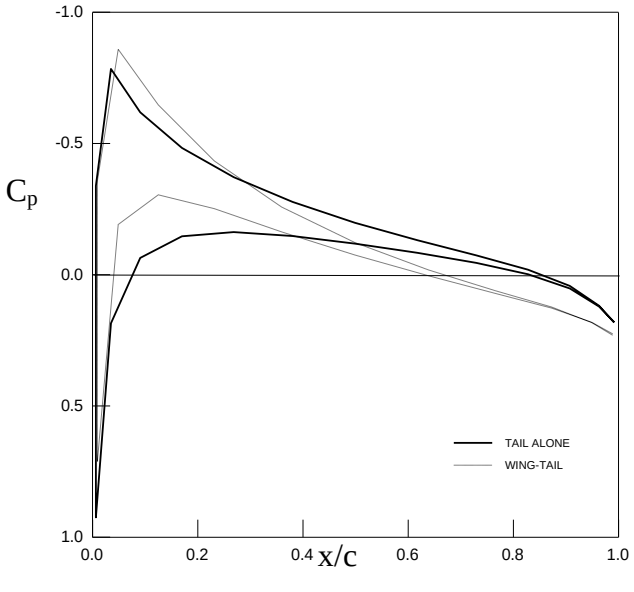

Fig (16): Pressure Distribution on the Tail at 2y/c=0.81.

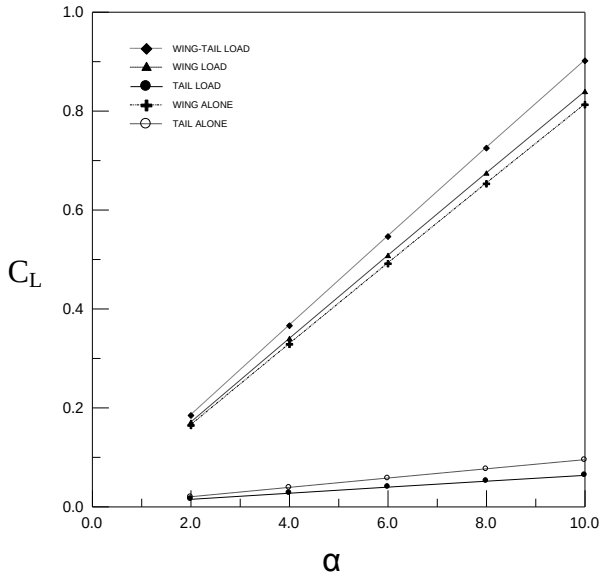

Fig (17): Wing-Tail Lift Coefficients with Angle of Attack.

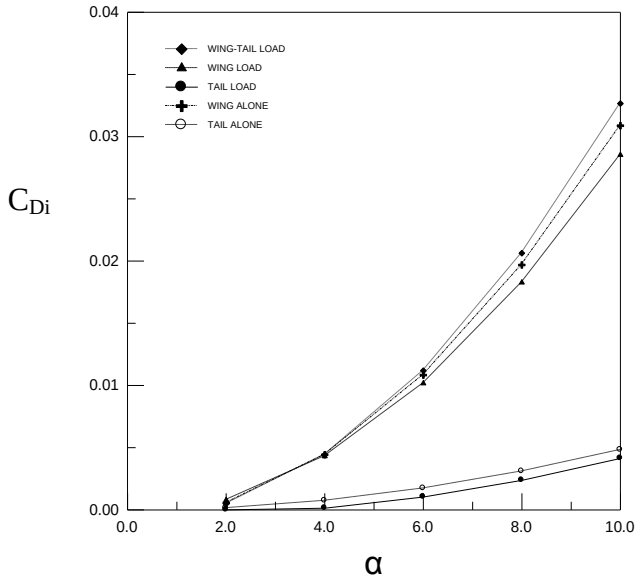

Fig (18): Wing-Tail Induced Drag Coefficients with Angle of Attack.

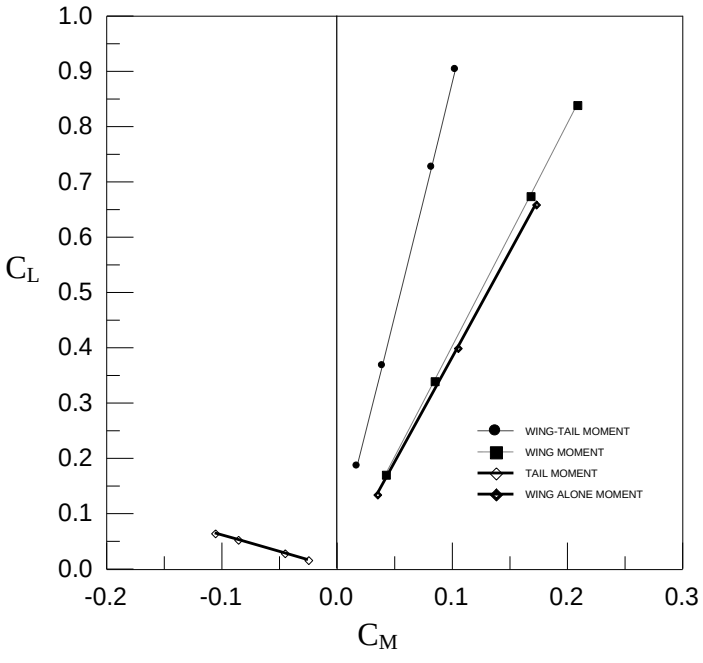

Fig (19): Wing-Tail Moment Coefficients with Lift Coefficient.

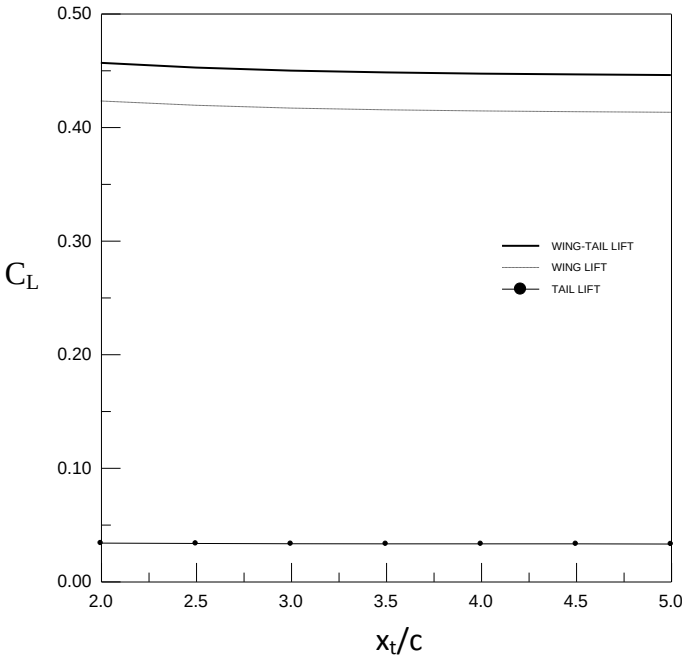

Fig (20): Wing-Tail Lift Coefficients with Distance Between Wing and Tail $\alpha=5^o$.

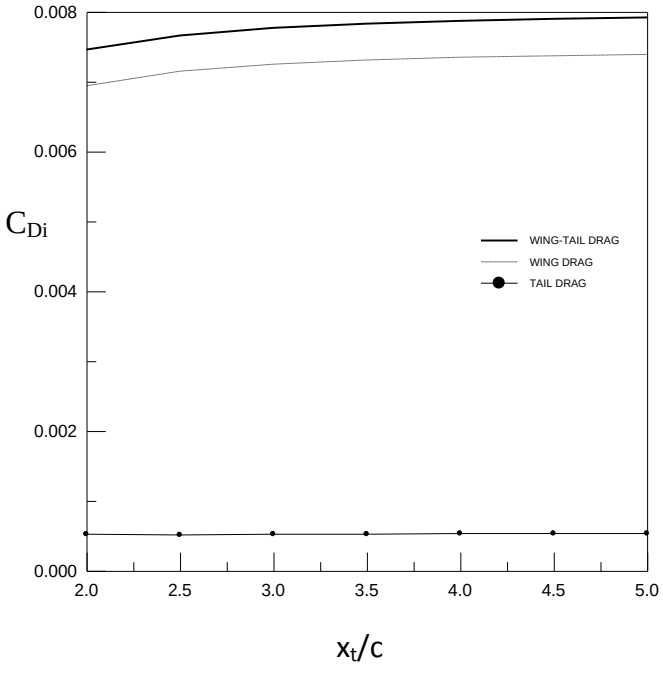

Fig (21): Wing-Tail Induced Drag Coefficients with Distance Between Wing and Tail, $\alpha=5^o$.

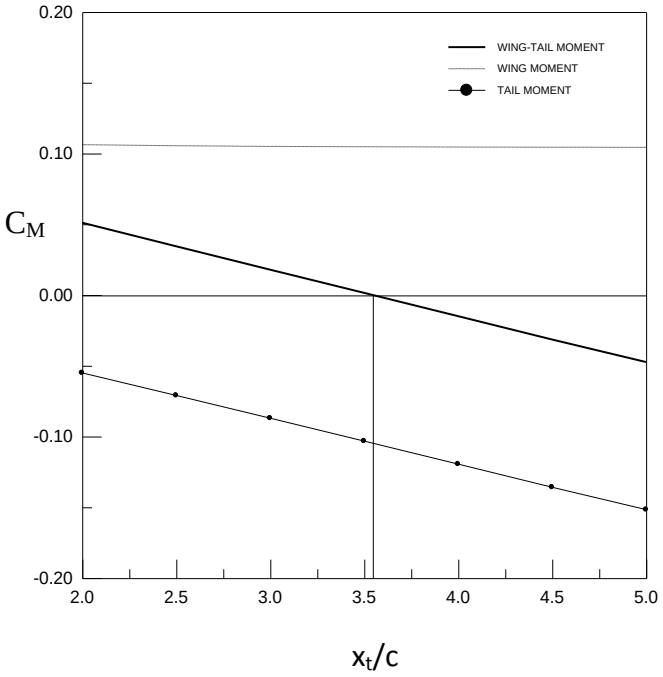

Fig (22): Wing-Tail Moment Coefficients with Distance Between Wing and Tail, $\alpha=5^o$.

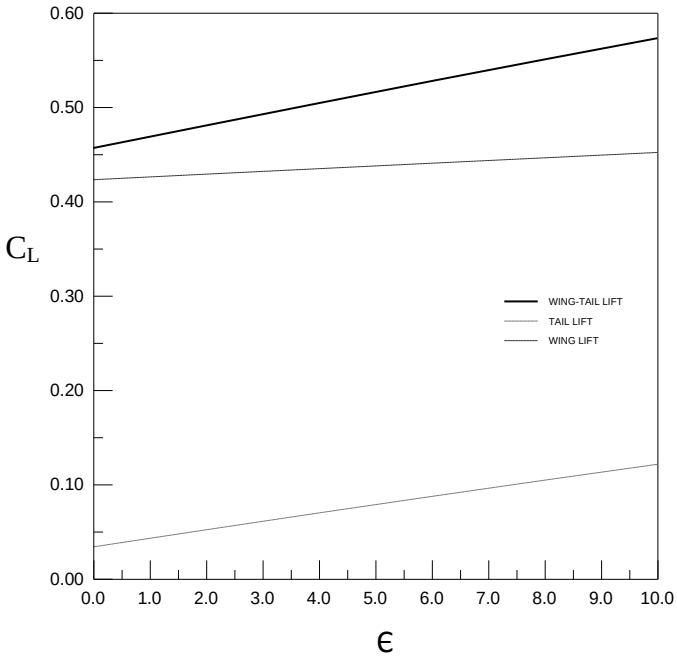

Fig (23): Wing-Tail Lift Coefficients with Tail Setting Angle, $\alpha=5^o$.

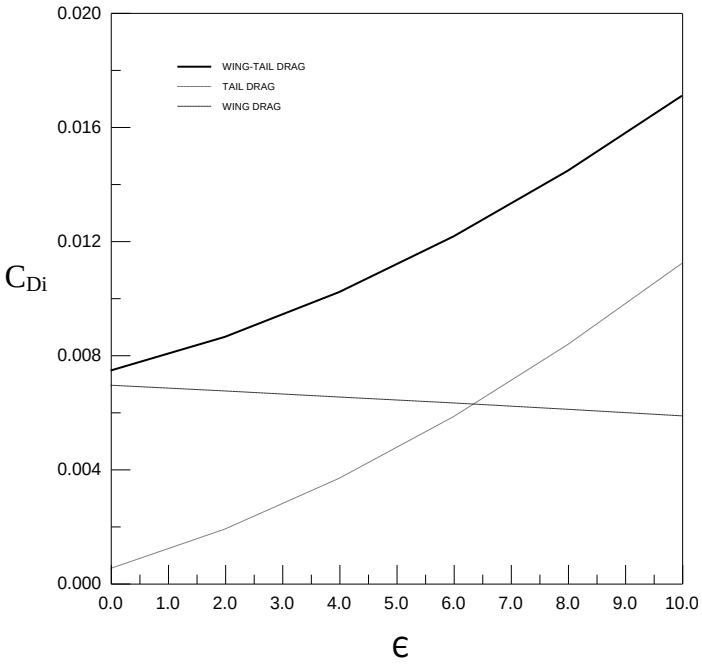

Fig (24): Wing-Tail Induced Drag Coefficients with Tail Setting Angle, $\alpha=5^o$.

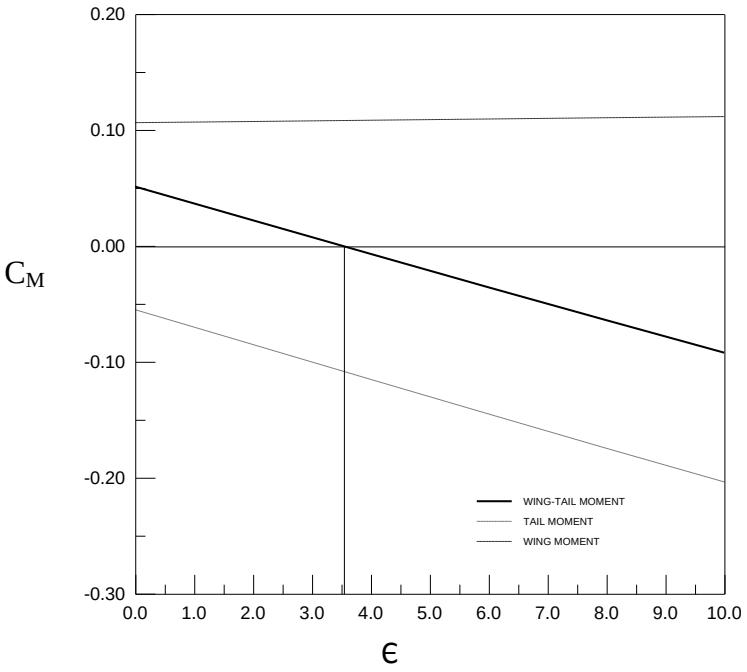

Fig (25): Wing-Tail Moment Coefficients with Tail Setting Angle, $\alpha=5^{o}$.